51st AIAA Aerospace Sciences Meeting including the New Horizons Forum and Aerospace Exposition
07 - 10 January 2013, Grapevine (Dallas/Ft. Worth Region), Texas

AIAA 2013-0864

# A Fully-Coupled Approach to Simulate Three-Dimensional Flexible Flapping Wings

Tao Yang*, Mingjun Wei†
*New Mexico State University, Las Cruces, NM 88003*

**In this study, a fully-coupled approach is used to simulate three-dimensional highly-flexible flapping wings interacting with the surrounding fluid flow. In this approach, the elastic body and its interaction with the fluid are implemented as body/surface force terms. In this way, the fluid and solid can be solved by a combined and modified form of typical Navier-Stokes equations. The motion trajectory is defined similarly by adding another bodyforce term using direct-forcing type of Immersed Boundary method. The advantage of solving a combined fluid-solid equation in a global Eulerian framework is that the solution of fluid, solid, and their interaction can be obtained in a monolithic manner and we avoid any sub-step iterations. The current extension of algorithm to three-dimensional configuration is based on our earlier work in two-dimensional setup. After extensive benchmarks in 2D and 3D, rigid and flexible cases, we eventually apply the algorithm on solving three-dimensional flexible flapping wings.**



## I. Introduction

Driven by the need for micro air vehicle (MAV) at bird/insect size, there is renewed interest in the study of flapping-wing motion for efficient flying at low Reynolds number [1]. Rigorous study of flapping motion can trace back to the pioneer work of Knoller [2] and Betz [3], who independently found the thrust generated by flapping wings. Since then, there have been many studies to understand the behavior of flapping-wing motion in ways analytically, numerically, and experimentally. Much of the insight into the mechanism of flapping flight has been contributed by various researchers: Garrick [4] showed that plunging airfoils produce positive thrust at all the frequencies, whereas pure pitching airfoils only produce thrust when the frequency is greater than a critical value; Jones, Dohring and Platzer have studied plunging airfoils and the vortex shedding using both numerical simulation and experiments [5], and they noticed an interesting vortex deflection at high plunging frequency, which were later investigated numerically in more details by Lewin and Haj-Hariri [6]; Anderson and his co-workers studied plunging, pitching, and the combined motion and discovered the highest propulsive efficiency at about 87% for some Strouhal number, angle of attack, and at an optimal phase angle between the pitching and plunging [7]; Buchholz and Smits have also investigated experimentally the wake and thrust of pitching plates with the focus on three-dimensional vortex structures appeared at high Strouhal number [8].

However, most of the earlier studies stayed for rigid wings, though the advantage of introducing flexibility to flapping wings has been widely noticed. From the numerical simulation point of view, the main difficulty to advance the study from rigid wings to flexible wings lies in the computational capability of fluid-solid interaction (FSI). To resolve a fully-coupled motion between solid

*Post-doctoral researcher, Department of Mechanical and Aerospace Engineering, Student Member AIAA
†Associate Professor, Department of Mechanical and Aerospace Engineering, Senior Member AIAA

structures and the surrounding fluid flow, sub-step interactions are often involved between the fluid solver and solid solver, or alternatively, the time-step needs to be very small to avoid iterations. So that, the algorithm can be entirely uneconomical or sometimes impossible for highly flexible three-dimensional configurations. In this paper, we are exploring a new approach to solve the FSI problems in a monolithic way and in a global Eulerian framework to obtain the computational efficiency and other conservation properties. The basic idea of solving a combined fluid-solid equation in Eulerian framework follows the FSI approach proposed by Zhao, Freund, and Moser [9]. The similar idea was proposed individually by Boffi et al. [10]. The current approach to solve three-dimensional problems is an extension of and based on our earlier work for two-dimensional problems [11].

In this paper, we first introduce the basic algorithm in §II, where some major challenges for three-dimensional implementation are also discussed. Then, in §III, we show some preliminary simulation results for a heaving flexible plate with low-aspect-ratio and a flexible plate under root flapping.



## II. Methodology

### II.A. Global Eulerian formulation for fluid and solid

The basic formulation for a combined description of fluid and solid is similar to the one used in our previous work for two-dimensional problems [11]. For completeness, the idea is briefly reviewed here. The FSI mechanism is based on the modified Navier-Stokes equations to describe both fluid and solid in an Eulerian point of view, which was firstly proposed by Zhao et al. [9]:

$$\frac{\partial \mathbf{u}}{\partial t} + \mathbf{u} \cdot \nabla \mathbf{u} = -\nabla p + \frac{1}{Re_f} \nabla^2 u + \nabla \cdot (\chi_s \boldsymbol{\tau}_{elas}) \tag{1}$$

with

$$\chi_s = \begin{cases} 1 & in \;\; Solid \\ 0 & otherwise \end{cases}, \tag{2}$$

where $\mathbf{u}$ is the velocity vector (in current three-dimensional Cartesian coordinate, $\mathbf{u} = (u, v, w)$), $\rho$ is the density and assumed the same for both fluid and solid, $Re_f$ is the typical Reynolds number based on fluid parameters with the same viscosity being assumed for both fluid and solid, and $\boldsymbol{\tau}_{elas}$ is the solid elastic stress with value only in the solid region. The elastic stress is calculated using simple neo-Hookean model,

$$\boldsymbol{\tau}_{elas} = \mu_s (\mathbf{A} \cdot \mathbf{A}^T - \mathbf{I}), \tag{3}$$

where $\mathbf{A}$ is the solid deformation gradient tensor and $\mu_s$ is the shear modulus.

The combined formulation (1) allows a global description of FSI problems with the interaction included seamlessly. However, to *flap* the wing, a mechanism for trajectory control needs to be implemented. As shown in our previous work for two-dimensional flapping wings [11], we defined control cells as *moving skeleton* (i.e. here, blue cells in figure 1), where another bodyforce term is defined by using the direct-forcing type of immersed boundary [12]. The combined equation with flapping mechanism now is

$$\frac{\partial \mathbf{u}}{\partial t} + \mathbf{u} \cdot \nabla \mathbf{u} = -\nabla p + \frac{1}{Re_f} \nabla^2 \mathbf{u} + \nabla \cdot (\chi_s \boldsymbol{\tau}_{elas}) + \chi_c f, \tag{4}$$

where $\chi_c$ only has non-zero value in the region of control parts, and $f$ is the direct forcing to achieve

the prescribed motion. The forcing term $f$ is defined by

$$f = \begin{cases} -(\text{RHS})^n + \frac{1}{\triangle t}(\mathbf{V} - \mathbf{u}^n) & in \quad the\ region\ of\ control\ parts \\ 0 & otherwise \end{cases}, \tag{5}$$

where the term RHS includes all right-hand-side terms for time advancement. The first-order time advancement is used here only for demonstration of the idea, and the actual algorithm is implemented for third-oder Runge-Kutta scheme with the same idea.

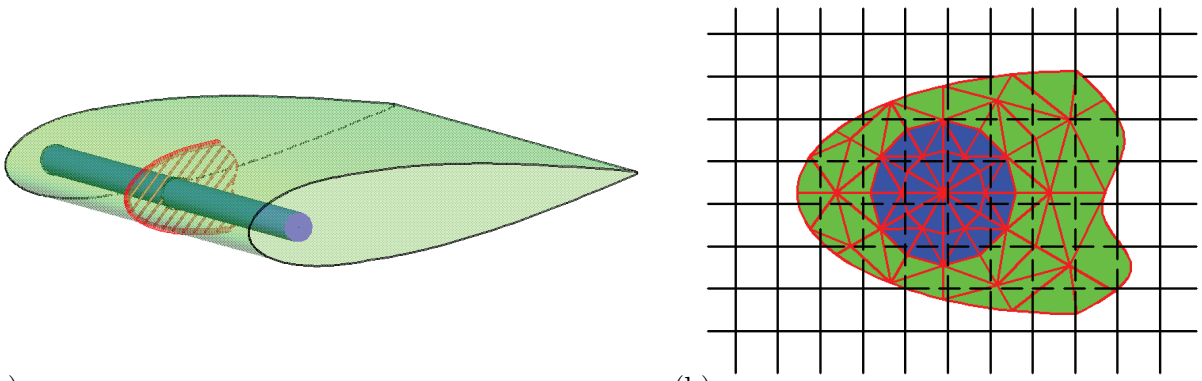

(a) (b)

**Figure 1. (a) The sketch of mesh configuration for a 3D NACA airfoil: the blue part is the contol part and the green part is the free solid which moves passively by fluid-solid interaction; (b) an cross section showing mesh details**

## II.B. Details for three-dimensional implementation

The implementation of the global algorithm to three-dimensional simulation is similar to the way used in two-dimensional simulations [11]. However, there are some complexities brought in by the extension to three-dimension, which are discussed in this section.

### *II.B.1. Information exchange between Eulerian coordinate and Lagrangian points*

The Lagrangian points for solid are continuously updated by the Eulerian velocity field calculated from (4), so that, the solid stress can be obtained by (3). However, the resulted solid stress field, which is discontinuous, needs to be smooth out before projecting back to the Eulerian description. As suggested by Zhao et al. in the original two-dimensional algorithm, Zienkiewiez-Zhu(ZZ) Patch can be used for this purpose. So, the ZZ Patch method in 3D is implemented here. Then, the continuous stress field needs to be projected to the Cartesian coordinate $(x, y, z)$. We use a simple trilinear interpolation as

$$\mathbf{f}_{ijk} = -\frac{1}{h_x h_y h_z} \int_{V_s} \nabla \psi_{ijk} \cdot \boldsymbol{\tau}_{elas} dV. \tag{6}$$

where $\psi_{ijk}$ are the trilinear interpolation coefficients defined by

$$\begin{aligned}
\psi_{i,j,k} &= (1-s_x)(1-s_y)(1-s_z),\\
\psi_{i+1,j,k} &= s_x(1-s_y)(1-s_z),\\
\psi_{i,j+1,k} &= (1-s_x)s_y(1-s_z),\\
\psi_{i,j,k+1} &= (1-s_x)(1-s_y)s_z,\\
\psi_{i+1,j+1,k} &= s_x s_y(1-s_z),\\
\psi_{i+1,j,k+1} &= s_x(1-s_y)s_z,\\
\psi_{i,j+1,k+1} &= (1-s_x)s_y s_z,\\
\psi_{i+1,j+1,k+1} &= s_x s_y s_z.
\end{aligned}$$

Figure 2 shows the notation for the trilinear interpolation.

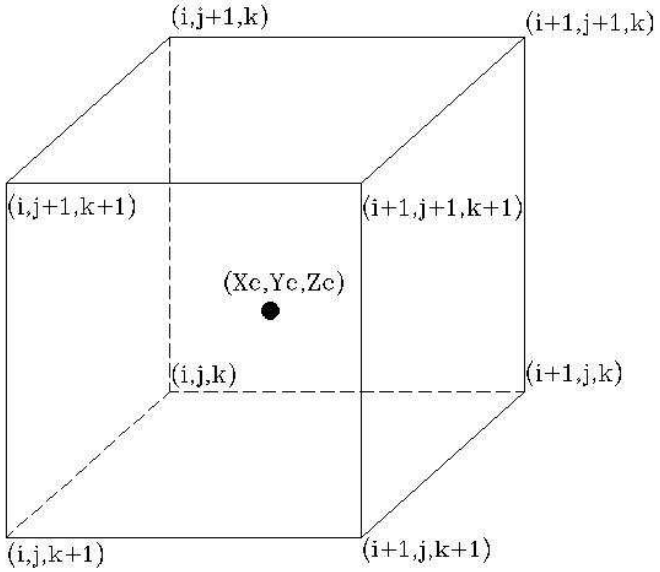


**Figure 2. The notation for trilinear interpolation**



### *II.B.2. Common refinement of solid cells*

To calculate the integration accurately during the projection, every Lagrangian solid cell is divided into several subelements which are confined within one single Cartesian mesh cell. In three-dimensional case, the Lagrangian cells are cut into subelements by using the Cartesian mesh faces parallel to $x-y$, $y-z$, and $x-z$ planes. The surfaces of these subelements are either part of the surfaces from Lagrangian cells or coinciding with the Cartesian mesh faces. Figure 3 shows an example of common refinement where the Lagrangian tetrahedron is divided into three subelements.

### *II.B.3. Gauss quadrature rule*

With the assumption that the solid stress field at arbitrary point $(x, y, z)$ inside the subelement can be approximated by

$$\boldsymbol{\tau} = \boldsymbol{a_0} + \boldsymbol{a_x}x + \boldsymbol{a_y}y + \boldsymbol{a_z}z,$$

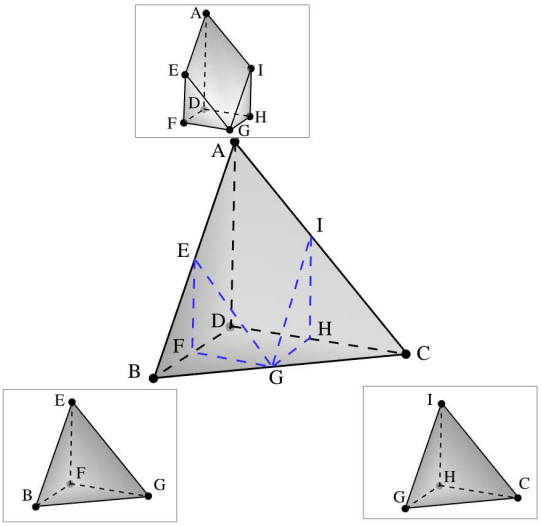


**Figure 3. An example of common refinement for three-dimensional solid cells**

the integration in (6) becomes a linear combination of polynomials $a_{lmn}x^l y^m z^n$ $(l+m+n \leq 4)$. Using Gauss theorem, we can change the volume integration to surface integration as

$$\int_{V_s} \sum (a_{lmn} x^l y^m z^n) dV = \int_{\partial V_s} \sum (a_{lmn} \frac{1}{l+1} x^{l+1} y^m z^n) n_x dS, \tag{7}$$

which then is computed by Gauss quadrature method,

$$\int_{\partial V_s} \sum (a_{lmn} \frac{1}{l+1} x^{l+1} y^m z^n) dS = \sum_{s_i} \left\{ A_i \sum_{iGq} \left\{ \left[ \sum (a_{lmn} \frac{1}{l+1} x^{l+1} y^m z^n) \right]_{iGq} w_{iGq} \right\} \right\} \tag{8}$$

## III. Applications

### III.A. Benchmark studies

#### *III.A.1. Rigid sphere*

First we study the flow around a stationary rigid sphere which has been investigated theoretically, numerically [13, 14] and experimentally [15, 16]. In our study, the nondimensional diameter of the sphere is $D = 1.0$, and the free stream velocity is constant, $u_\infty = 1.0$. The dynamic viscosity of fluid $\mu_f$ is changed for different values of Reynolds number $R_e = \rho u_\infty D/\mu_f$. The cases with different values of Reynolds number, $R_e = 50, 100, 150, 200, 250$ and 300, are studied.

We compare the wake pattern in the downstream for different Reynolds number with the results from [14]. For cases with low Reynolds number, $R_e = 50, 100, 150$ and 200, the downstream flow is axisymmetric. Figure 4 shows the vorticity contours for such axisymmetric flow. For $R_e = 250$ and 300, the flow becomes unsymmetric, and hairpin vortex appears when $R_e = 300$, which is shown in figure 5. It is shown that our results match well with others' qualitatively.

Also quantitative studies are made, e.g. drag coefficient. The drag coefficient $C_d = F_d/(0.5 * \rho U_\infty^2 D)$ for different Reynolds number is calculated by using control volume method and copmpared with numerical results [14] and experimental results [15], which provides good quantitative validation as shown in figure 6.

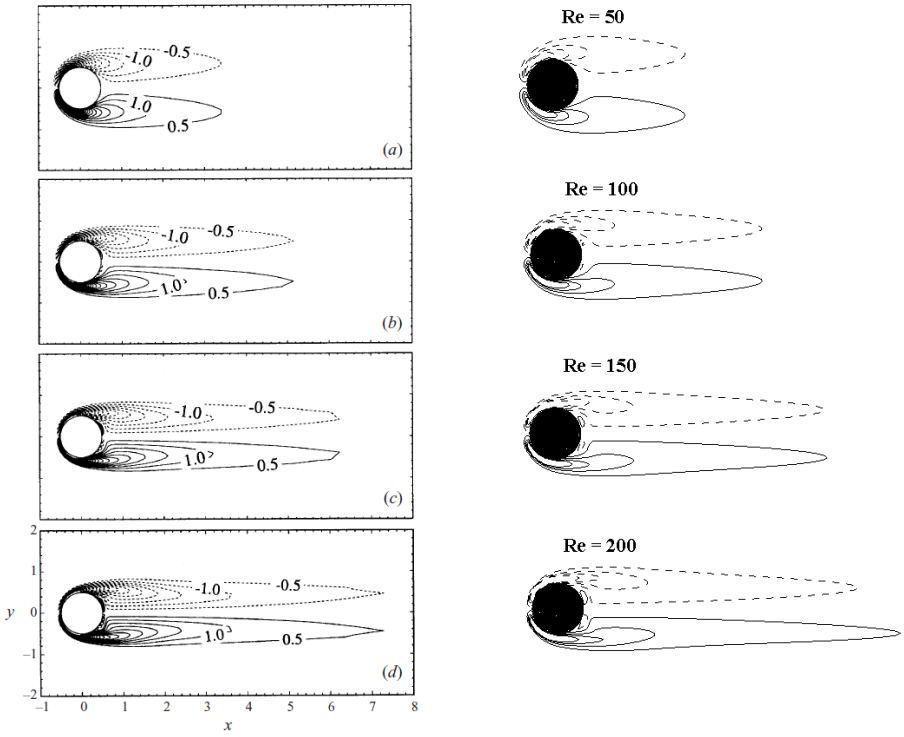


**Figure 4. Results of flow around a sphere for $R_e = 50, 100, 150$ and 200: left: results in [14], right: our simulation.**

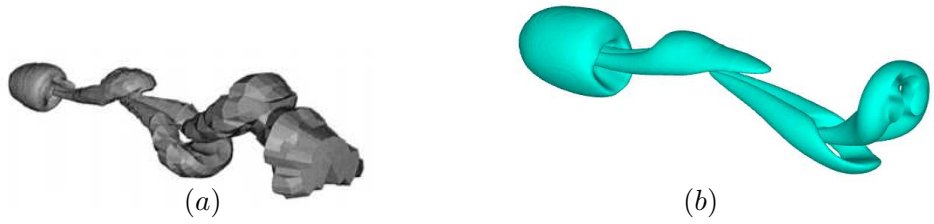


**Figure 5. Hairpin vortex for flow around a sphere with $R_e = 300$: (a) results in [14], (b) our simulation.**

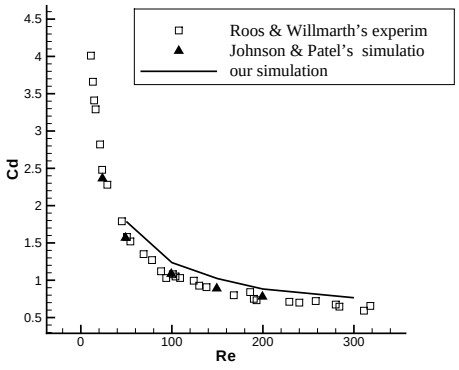


**Figure 6. Comparison of drag coefficient for flow past a sphere with different Reynolds number.**



*III.A.2. Viscoelastic particle*

We also investigate a two-dimensional floppy viscoealstic particle in shear flow and compare our results with those in [17, 18].

With the assumption that $\rho_f = \rho_s$, the governing equation for this problem can be written as

$$\frac{\partial \mathbf{u}}{\partial t} = -\nabla p + \frac{1}{Re_f}\nabla^2 \mathbf{u} + \nabla \cdot (\chi_s \boldsymbol{\tau}_{elas}) \tag{9}$$

where $\boldsymbol{\tau}_{elas}$ is the stress term based on neo-Hookean model (3). Here, we neglect the inertia term because Reynolds number, $Re = \rho \dot{\gamma} a^2/\mu_f$ which is based on shear rate $\dot{\gamma}$ and particle radius $a$, is very small in our studies.

Figure 7 shows the sketch of our simulation. In our studies, the Couette flow is chosen as the shear flow. For different values of initial aspect ratio and Capillary number $C_a = \dot{\gamma}\mu_f/\mu_s$, there are three types of motion: tank-treading, swinging(trembling) and tumbling, as shown in figure 8.

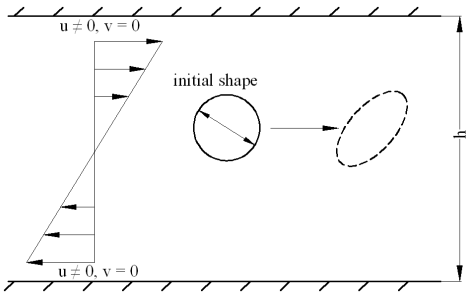


**Figure 7. The sketch of a viscoelastic particle in shear layer flow.**

In our studies, we investigated the effects of Capillary number and aspect ratio. For each aspect ratio, a critical Capillary number exists, which separates region of trembling motion and tumbling motion. Figure 9 shows the regions of trembling motion and tumbling motion. The comparison indicates that our approach works well for fluid-structure interaction problems.

## III.B. Simulations

We have applied the fully-coupled approach to simulate three-dimensional flexible flapping wings.

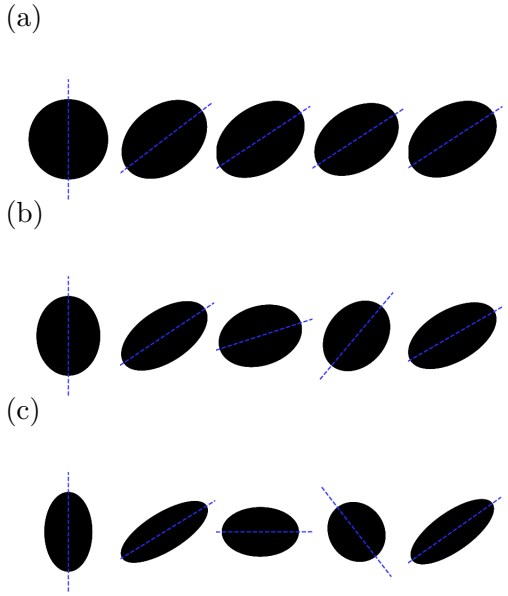


**Figure 8. Different types of motion of viscoelastic particle in shear flow: (a) Tank-treading, (b) Trembling, (c) Tumbling.**

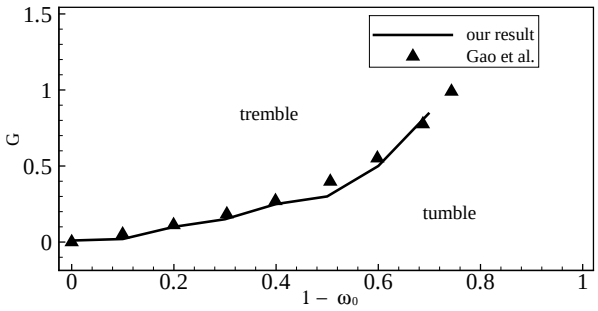


**Figure 9. Regions of trembling motion and tumbling motion for two-dimensional viscoelastic particle in shear flow.**

The computation domain is a volume area with $-1 < x < 3$, $-1 < y < 1$ and $0 < z < 2$, and mesh size $200 \times 100 \times 100$ is used for all the simulations. Uniform staggered-mesh is used in Eulerian framework, and quadratic tetrahedron cells are picked up for Lagrangian mesh.

The wing model used in our simulation is based on the measurement from a flying bat toy as shown in figure 10. Figure 10 shows the wing from the flying bat toy and the single-layer model used in the studies. The blue part is the "skeleton" part with prescribed motion, while the green part moves passively(sketched in figure 11). The left blue part is fixed and the right blue part has a prescribed rotation motion.

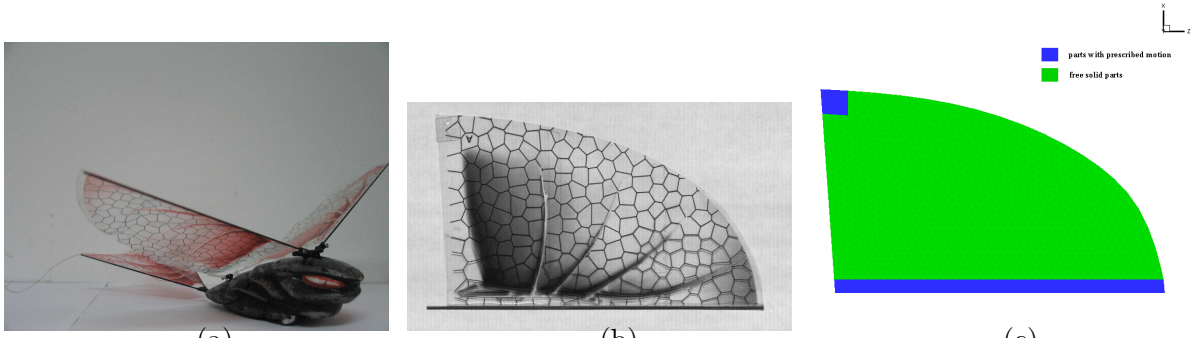


(a) (b) (c)

**Figure 10. Real and model wings: (a) toy from manufactured by *Interactive Toy Concepts Ltd.*, (b) Real wing from the toy, (c) single-layer curve wing model in our simulations.**

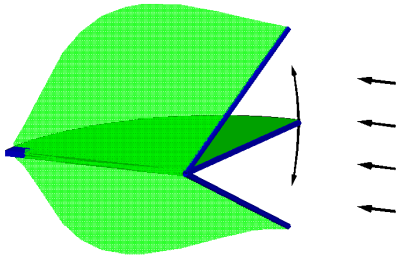

**Figure 11. The sketch for simulations of three-dimensional flexible flapping wings.**

In our studies, we simulate two cases with different values of angle of attack $\alpha$: 1) $\alpha = 0°$; 2) $\alpha = 14°$. The prescribed rotation motion can be expressed by

$$\theta = \frac{a}{L}\sin(2.0K\pi t) + \theta_0, \tag{10a}$$

$$\omega = \frac{2.0aK\pi}{L}\cos(2.0K\pi t) \tag{10b}$$

where $a = 0.1$, $K = 1.0/\pi$, $L = 18/(19.5\pi)$ and $\theta_0 = 10.5°$, which are measured from the toy.

Results are shown below in figure 12 and 13 for $\alpha = 0°$ and $\alpha = 14°$ respectively, where vortex structures are marked by Q-criterion and zoom-in pictures at the bottom are to show the details of structural deformation which are painted by normal stress and shear stress respectively. For both cases, two vortex streets are observed. At $\alpha = 0°$, the two vortex street are close to each other, when we increase the angle of attack to $\alpha = 14°$, they move away from each other. And it is observed that the normal stress and shear stress increase as the angle of attack increases.

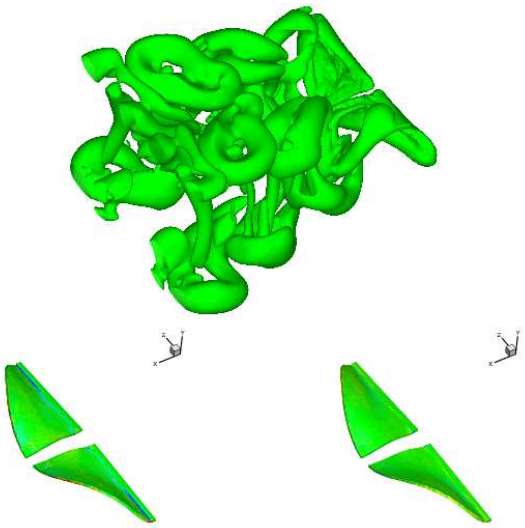

**Figure 12. The result of three-dimensional flexible flapping wings with angle of attack $\alpha = 0°$: (top) vortex structures shown by Q-criterion, (bottom) zoom-in pictures showing the details of structural deformation which are painted by (left) $\tau_{xx}$ and (right) $\tau_{yy}$.**

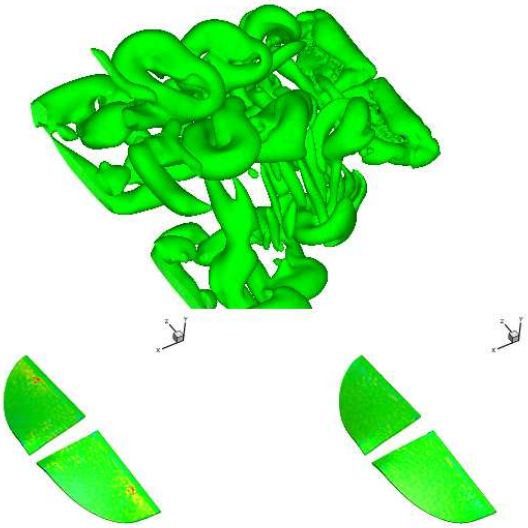

**Figure 13. The result of three-dimensional flexible flapping wings with angle of attack $\alpha = 14°$: (top) vortex structures shown by Q-criterion, (bottom) zoom-in pictures showing the details of structural deformation which are painted by (left) $\tau_{xx}$ and (right) $\tau_{yy}$.**

## IV. Conclusions

In this paper, we developed a strong-coupling approach with immersed boundary method to simulate three-dimensional fluid-structure interaction problems. The unified formula in Eulerian framework for both fluid and solid are introduced. Details of numerical algorithm, including force-projection method, "cell division technique" and Gauss quadratic rule, were discussed.

Then we validated our approach by comparing our results with those from other simulations and experiments for two cases: flow around rigid stationary sphere and two-dimensional floppy viscoelastic particle in shear flow. All the qualitative and quantitative studies showed that our results matched very well with the referred results.

The fully-coupled approach was also applied on three-dimensional flexible flapping wings with different values of angle of attack. From the results, it was observed that different angle of attack leads to different vortex structures. The two vortex street in the wake flow move away from each other when the angle of attack is increased.



## Acknowledgment

The authors would gratefully acknowledge the support by Army Research Laboratory through Army High Performance Computing Research Center (AHPCRC) and through Micro Autonomous Systems and Technology (MAST) Collaborative Technology Alliance (CTA).

## References

[1]Mueller, T. J. and DeLaurier, J. D., "An overview of Micro Air Vehicle aerodynamics," *Fixed and Flapping Wing Aerodynamics for Micro Air Vehicle Applications*, edited by T. J. Mueller, American Institute of Aeronautics and Astronautics, Inc., 2001.

[2]Knoller, R., "Die Gesetze des Luftwiderstandes," *Flug- und Motortechnik (Wien)*, Vol. 3, No. 21, 1909, pp. 1–7.

[3]Betz, A., "Ein Beitrag zur Erklärung des Segelfluges," *Zeitschrift für Flugtechnik and Motorluftschiffahrt*, Vol. 3, 1912, pp. 269–272.

[4]Garrick, I. E., "Propulsion of a flapping and oscillating airfoil," NACA Rept. 567, 1936.

[5]K. D. Jones, C. M. D. and Platzer, M. F., "Experimental and Computational Investigation of the Knoller-Betz Effect," *AIAA J.*, Vol. 36, No. 7, 1998, pp. 1240–1246.

[6]Lewin, G. C. and Haj-Hariri, H., "Modelling thrust generation of a two-dimensional heaving airfoil in a viscous flow," *J. Fluid Mech.*, Vol. 492, 2003, pp. 339–362.

[7]Anderson, J. M., Streitlien, K., Barrett, D. S., and Triantafyllou, M. S., "Oscillating foils of high propulsive efficiency," *J. Fluid Mech.*, Vol. 360, 1998, pp. 41–72.

[8]Buchholz, J. H. J. and Smits, A. J., "The wake structure and thrust performance of a rigid low-aspect-ratio pitching panel," *J. Fluid Mech.*, Vol. 603, 2008, pp. 331–365.

[9]Zhao, H., Freund, J. B., and Moser, R. D., "A fixed-mesh method for incompressible flow-structure systems with finite solid deformations," *J. Comput. Phys.*, Vol. 227, 2008, pp. 3114–3140.

[10]Boffi, D., Gastaldi, L., Heltai, L., and Peskin, C. S., "On the hyper-elastic formulation of the immersed boundary method," *Computer Methods in Applied Mathematics and Engineering*, Vol. 197, 2008, pp. 2210–2231.

[11]Yang, T., Wei, M., and Zhao, H., "Numerical study of flexible flapping wing propulsion," *AIAA J.*, Vol. 48, No. 12, 2010, pp. 2909–2915.

[12]Mohd-Yusof, J., "Combined immersed-boundary/B-spline methods for simulations of flow in complex geometries," Center for Turbulence Research, Annual Research Briefs – 1997, 1997.

[13]Kim, I. and Pearlstein, A. J., "Stability of the flow past a sphere," *J. Fluid Mech.*, Vol. 211, 1990, pp. 73–93.

[14]Johnson, T. A. and Patel, V. C., "Flow past a sphere up to a Reynolds Number of 300," *J. Fluid Mech.*, Vol. 378, 1999, pp. 19–70.

[15]Roos, F. and Willmarth, W. W., "Some experimental results on sphere and disk drag," *AIAA J.*, Vol. 9, No. 2, 1971, pp. 285–291.

[16]Szaltys, P., Chrust, M., Przadka, A., Goujon-Durand, S., Tuckerman, L., and Wesfreid, J., "Nonlinear evolution of instabilities behind spheres and disks," *Journal of Fluids and Structures*, Vol. 28, 2012, pp. 483–487.

[17]Gao, T., Hu, H. H., and Castaneda, P. P., "Rheology of a suspension of elastic particles in a viscous shear flow," *J. Fluid Mech.*, Vol. 687, 2011, pp. 209–237.

[18]Gao, T., Hu, H. H., and Castaneda, P. P., "Shape dynamics and rheology of soft elastic particles in a shear flow," *Computer Methods in Applied Mathematics and Engineering*, Vol. 108, No. 5, 2012.